J Nanopart Res (2016)18:311
DOI 10.1007/s11051-016-3538-3

RESEARCH PAPER

A pyrazolyl-based thiolato single-source precursor for the selective synthesis of isotropic copper-deficient copper(I) sulfide nanocrystals: synthesis, optical and photocatalytic activity

Gopinath Mondal · Ananyakumari Santra · Pradip Bera · Moumita Acharjya · Sumanta Jana · Dipankar Chattopadhyay · Anup Mondal · Sang Il Seok · Pulakesh Bera

Received: 17 March 2016 / Accepted: 27 July 2016

Abstract Hexagonal copper-deficient copper(I) sulfide ($Cu_{2-x}S$, $x = 0.03$, 0.2) nanocrystals (NCs) are synthesized from a newly prepared single-source precursor (SP), $[Cu(bdpa)_2][CuCl_2]$, where bdpa is benzyl 3,5-dimethyl-pyrazole-1-carbodithioate. The SP is crystallized with space group $P\bar{1}$ and possesses a distorted tetrahedron structure with a CuN_2S_2 chromophore where the central copper is in +1 oxidation state. Distortion in copper(I) structure and the low decomposition temperature of SP make it favorable for the low-temperature solvent-assisted selective growth of high-copper content sulfides. The nucleation and growth of $Cu_{2-x}S$ ($x = 0.03$, 0.2) are effectively controlled by the SP and the solvent in the solvothermal decomposition process. During decomposition, fragment benzyl thiol ($PhCH_2SH$) from SP effectively passivates the nucleus leading to spherical nanocrystals. Further, solvent plays an important role in the selective thermochemical transformation of Cu^I-complex to $Cu_{2-x}S$ ($x = 0.03$, 0.2) NCs. The chelating binders (solvent) like ethylene diamine (EN) and ethylene glycol (EG) prefer to form spherical $Cu_{1.97}S$ nanoparticles (djurleite), whereas nonchelating hydrazine hydrate (HH) shows the tendency to furnish hexagonal platelets of copper-deficient $Cu_{1.8}S$. The optical band gap values (2.25–2.50 eV) show quantum confinement effect in the structure. The synthesized NCs display excellent catalytic activity (~87 %) toward photodegradation of organic dyes like Congo Red (CR) and Methylene Blue (MB).

Electronic supplementary material The online version of this article (doi:10.1007/s11051-016-3538-3) contains supplementary material, which is available to authorized users.

G. Mondal · A. Santra · P. Bera · M. Acharjya · P. Bera (✉)
Post Graduate Department of Chemistry, Panskura Banamali College, Vidyasagar University, Midnapore (E), West Bengal 721152, India
e-mail: pbera.pbc.chem@gmail.com

G. Mondal · S. Jana · A. Mondal
Department of Chemistry, Indian Institute of Engineering Science and Technology (IIEST), Shibpur, West Bengal 711103, India

D. Chattopadhyay
Department of Polymer Science and Technology, University of Calcutta, 92 Acharya Prafulla Chandra Road, Kolkata 700009, India

S. I. Seok
KRICT-EPFL Global Research Laboratory, Division of Advanced Materials, Korea Research Institute of Chemical Technology, 141 Gajeong-Ro, Yuseong-Gu, Daejeon 305-600, South Korea

S. I. Seok
Department of Energy Science, Sungkyunkwan University, Suwon 440-746, South Korea

Published online: 17 October 2016

Keywords Solvothermal · Isotropic · Copper(I) sulfide · Nanocrystals · Photocatalytic activity

Introduction

In the past few decades, there has been an increasing interest to synthesize the semiconducting metal chalcogenide nanocrystals (NCs), because of their various applications in nanoscience and nanotechnology. Among the known metal sulfide semiconductors, copper sulfide is one of the most important candidate owing to varied morphologies, the presence of copper vacancies in the lattice, and wide stoichiometric compositions. The stoichiometric composition of copper sulfide varies in a wide range from copper-rich chalcocite (Cu_2S) to copper-deficient covellite (CuS) (Jiang et al. 2000). Vacancies (*p* type) in the crystal lattice of copper sulfide make them important for the potential applications in solid-state solar cells (Reijnen et al. 2003; Lin and Lee 2011; Wu et al. 2008), nonvolatile memory devices (Sakamoto et al. 2003; Chen et al. 2007), gas sensing (Sagade et al. 2009), and lithium ion batteries (Zhao et al. 2012). A large effort has been focused on controllable synthesis of copper sulfide crystallites with hierarchical microstructures and morphologies that include plate-like (Yan et al. 2008; Gonçalves et al. 2008), tubular (Wu et al. 2006; Lu et al. 2002; Gong et al. 2006), spherical (He et al. 2007), flower-like (Thongtem et al. 2009), rod-like (Roy and Srivastava 2007), flake-like structures (Zhang et al. 2010) and so on. Various synthetic methods such as sonochemical (Wang et al. 2002), sol–gel (Malyarevich et al. 2000), hydrothermal (Roy and Srivastava 2006), solvothermal (Gorai et al. 2005), microemulsion (Haram et al. 1996), and electrodeposition (Ghahremaninezhad et al. 2011) etc., have been employed to prepare copper sulfide NCs. Most of these methods require high temperature, toxic surfactants, and purification of the final products. Recently, the development of various single-source precursors (SPs) and their uses in the synthesis of hierarchical structure with controllable shape, size, and crystallinity following solvothermal decomposition has been popularized (Lai et al. 2012). Tuning topology for the synthesis of NCs could be maintained in the structure of SP during solvothermal decomposition. Solvothermal SP route also offers the advantages of mildness, safety, simplified cost-effective synthesis of NCs over the other reported methods. Moreover, toxic surfactants need not be used in the reaction medium. The presence of all constituents in required atomic ratio is chemically maintained in the SP method to prepare selective product. Metal diethyldithiocarbamate has been used to synthesize a wide range of metal sulfides including copper sulfide NCs (Shen et al. 2011). Korgel et al. synthesized Cu_2S nanorods, nanodisks, and nanoplatelets by solventless thermolysis of a copper-alkylthiolato precursor (Sigman et al. 2003; Larsen et al. 2003). Liu et al. decomposed $Cu(S_2CNEt_2)_2$ in a mixture of dodecanethiol and oleic acid to obtained hexagonal wires of Cu_2S (chalcocite) (Liu et al. 2005). The same precursor is thermolyzed in trioctylphosphine and trioctylphosphine oxide (TOP/TOPO) to obtain spherical $Cu_{1.8}S$ (digenite) nanocrystals (Lou et al. 2007). Corncob-like Cu_2S nanostructures were obtained through thermolysis of copper dithiolate in dodecanethiol (Du et al. 2006). Li et al. also reported a facile synthesis of monodispersed Cu_2S nanocrystals by the reaction of Cu(II)-stearate and dodecanethiol in 1-octadecene (Li et al. 2009). Most of these synthetic methods associate with the use of templates or surfactants agent which are most hazardous materials for environmental pollution. Very recently, the Liberato Manna group use Cu(I) complexes to prepare copper-rich platelet of copper sulfide nanoparticles (Xie et al. 2013). The Cu:S ratio could be increased retaining the overall size and morphology of the product. It was also argued that various ligands internally act as structure-directing agent in the growth of NCs. So, the ligand structure along with the coordination environment of the metal plays an important role in determining the phase, morphology, and size of the particles (Nair and Scholes 2006). Uses of predesigned heterocycle-based ligand for the synthesis of SP are reported in the preparation of high-quality metal sulfide NCs (Nyamen et al. 2011, 2013; Mthethwa et al. 2009). We reported earlier the solvothermal decomposition of N-heterocyclic copper(I) complex for the selective synthesis of hexagonal Cu_2S in ethylene glycol (EG) and ethylene diamine (EN) (Mondal et al. 2014; Bera et al. 2010). It was concluded that the SP with Cu(I) in its coordination had total control to the product stoichiometry. Here in this report the use of another Cu(I)-complex of benzyl

3,5-dimethyl-pyrazole -1-carbodithioate has been used as SP for the synthesis of copper-deficient copper(I) sulfides, $Cu_{2-x}S$ ($x = 0.03$, 0.2), following a low-temperature decomposition method in coordinating solvents like ethylene glycol (EG), ethylene diamine (EN), and hydrazine hydrate (HH) (Bera et al. 2010). A rational growth mechanism is also proposed. The photocatalytic activities of the synthesized copper-deficient copper(I) sulfide were checked toward the degradation of Congo Red (CR) and Methylene Blue (MB) dyes in visible light.

Experimental details

Copper chloride (Merck), acetyl acetone (Spectrochem), ethylene diamine (Himedia), ethylene glycol (Himedia), and hydrazine hydrate (Merck) were all of analytical grade and used without further purification. Solvent ethanol (Changshu Yangyuan Chemical, China), acetonitrile (Merck), and methanol (Merck) were dried and distilled before use.

Benzyl-3,5-Dimethyl-pyrazole-1-carbodithioate (bdpa) was prepared by a literature procedure (Mondal et al. 2015). 1 mmol, 0.170 g of $CuCl_2{\cdot}2H_2O$ methanolic (10 mL) solution was mixed with 1 mmol, 0.262 g of crystalline bdpa in 20 mL acetonitrile solvent in magnetic stirrer for 1 h at room temperature. After 1 h, a deep blue solid was precipitated out and filtered off, which was then washed with methanol–acetonitrile mixture. The product is dried in vacuum over silica gel and after 3–4 days, a dark blue single crystal was separated out from the filtrate part. Yield 80 %, Mass m/z: 587.10, 325.05. Anal. Calc. for $C_{26}H_{28}Cl_2Cu_2N_4S_4$: C, 43.20; H, 3.90; N, 7.75; S, 17.75. Observed: C, 43.16; H, 3.85; N, 7.70; S, 17.78.

In a typical synthetic process, 0.361 g (0.5 mmol) of precursor, $[Cu(bdpa)_2][CuCl_2]$, was taken with 15 mL of solvent in a 50-mL two-necked round bottom flask placed with a condenser and thermocouple adaptor. The flask was degassed at room temperature for 5 min and then filled with inert nitrogen gas. The resulting solution was then gradually heated up to 180 °C in the solvent and the heating is continued for another 60 min maintaining the same reaction temperature where upon a black crystalline product separated out. The black precipitate was collected through centrifugation and washed four to five times with dry ethanol. Dry powder of copper sulfide NCs was collected by evaporating ethanol at 100 °C for 2 h in vacuum oven. The reaction parameters and sample properties are given in Table 1.

Copper(I) sulfide NCs were synthesized by solvothermal process using coordinating solvents like EN, EG, and HH from a newly synthesized molecular precursor and the detailed procedure is given in the experimental section. The FTIR spectra (4000–400 cm^{-1}) were recorded on a Perkin Elmer Spectrum Two spectrophotometer. The samples were prepared using KBr pellets technique. The thermogravimetry (TG) analysis of precursor was carried out on Perkin Elmer TGA 4000 instrument at a heating rate 10 C/min under nitrogen. UV–Visible absorption spectra were recorded on a Perkin Elmer Lambda 35 spectrophotometer in 200–1000 nm wavelength range at room temperature and photo catalytic activity was observed under 250 W electric lamp. Powder X-ray diffraction (XRD) of the NCs was recorded using a Seifert XDAL 3000 diffractometer using graphite-monochromated Cu-Kα radiation ($\lambda = 1.5418$ Å) with a scan rate 5°/min over a range of $5° < 2\theta < 80°$ with steps of 0.02°, and the scintillation detector is operated at 40 kV and 40 mA. TEM and HRTEM of cadmium sulfide nanocrystals were characterized using a JEOL JEM–2100F EMI7220019 at an accelerating voltage of 200 kV. TEM samples were prepared by placing a drop of a dilute ethanol dispersion of nanocrystals on the surface of a 200-mesh carbon-coated copper grid. The SEM analyses of the samples were performed in a ZEISS EVO MA10 scanning electron microscope. Energy-dispersive X-ray (EDX) analyses of the samples were carried out on Oxford instrument INCA attached to the SEM in the scanning range of 20 keV. The samples were prepared by fixing the finely powder material on the surface of a carbon tape. XPS was performed on an AXIS NOVA X-ray photoelectron spectroscopy, using monochromatic Al-Kα radiation with an anode voltage of 15 kV, emission current of 10 mA, the low-resolution survey spectrum was recorded with a pass energy of 160 eV, high-resolution spectrum was recorded with a pass energy of 20 eV, and the quantification was calculated by peak area measurement. Photocatalytic activity of copper sulfide nanoparticles was studied with a 50 mL of 5×10^{-5} M and 6.2×10^{-5} M aqueous solutions of RB and MB, respectively, in a 100 mL beaker using visible light source. A 250 W indoor fluorescent lamp (Philips) was used as a light source. A 15 cm distance is maintained between lamp and reaction bath. All the experiments were performed at room temperature (25 °C).

Table 1 Reaction parameters and sample properties

Solvents	Temp. (°C)	Time (min)	Shape	Average size* (nm)	Phase
EN	180	60	Spherical	17	$Cu_{1.97}S$
EG	180	60	Spherical	16	$Cu_{1.97}S$
HH	180	60	Hexagonal	60[a]/40[b]	$Cu_{1.8}S$

[a] Length

[b] Breadth

* Calculated from TEM pictures

The concentration of the dye after photocatalyst degradation was determined with a Perkin Elmer Lambda 35 UV–Vis spectrophotometer.

Results and discussion

In an objective to synthesize copper(I) sulfide NCs, a copper(I) complex is designed and synthesized so that the Cu:S ratio is chemically maintained within the complex precursor. To stabilize lower oxidation state of copper, i.e., Cu(I), one kind of pyrazole-based ligand is considered. Pyrazole being isomeric with imidazole has suitable low lying vacant π* orbital to reduce the electron cloud of the central metal ion through Cu → π* orbital of L (ligand) back bond formation. Further, the sulfur group attached to pyrazole provides a reducing environment to stabilize Cu(I) complex.

To confirm the bonding mode of the ligand, we compare the IR spectra of the free ligand and the copper complex. Figure 1 represents the IR spectra of the ligand bdpa and its copper complex. The ligand shows the significant bands at 1572, 1422, 1272, 1171, 1022, and 787 cm^{-1} which can be assigned for symmetric vibrations of C = N, mixed vibration of (C–N) + (C–C), vibration of C–N, C–N–N, N–N, and C = S bond, respectively. The respective vibration of the bands of the ligand moiety appeared at 1588, 1453, 1319, 1131, 1022, and 733 cm^{-1} in the complex (Fig. 1b). An increase in υ(C = N) in the free ligand spectrum by ca. $\Delta\upsilon = 16$ cm^{-1} on complex formation [υ(C = N) = 1588 cm^{-1} in complex] and also increase in υ(C–N) in the free ligand spectrum by ca. $\Delta\upsilon = 31$ cm^{-1} [υ(C–N) = 1453 cm^{-1} in complex] indicate a coordination through tertiary pyrazole ring nitrogen atom. The coordination of thione (C = S) sulfur atom to metal center is indicated by a decrease of the υ(C = S) band from 787 cm^{-1} (in free ligand) to 733 cm^{-1} in its complex (Bera et al. 2008; Ali et al. 2012).

X-ray crystal structure determination of the SP confirms the points of attachments and the composition as $[Cu(bdpa)_2][CuCl_2]$. The detail of the structural characterization is under review and will appear shortly in a pure chemistry-based journal. The ORTEP diagram with atom numbering scheme is shown in Fig. 2 to visualize the SP structure as a ready reference. In geometry of SP, Cu(I) is tetrahedrally coordinated by the ternary N-atom and thione sulfur of two ligands and $CuCl_2$ unit is present outside the coordination sphere as cocrystal which satisfies the formal charge. The presence of the large benzyl group in the ligand ascertained a high order of distortion in the complex which becomes an effective SP for copper sulfide nanoparticles. Additionally, the crystal contains one $CuCl_2$ as the counter crystal part which

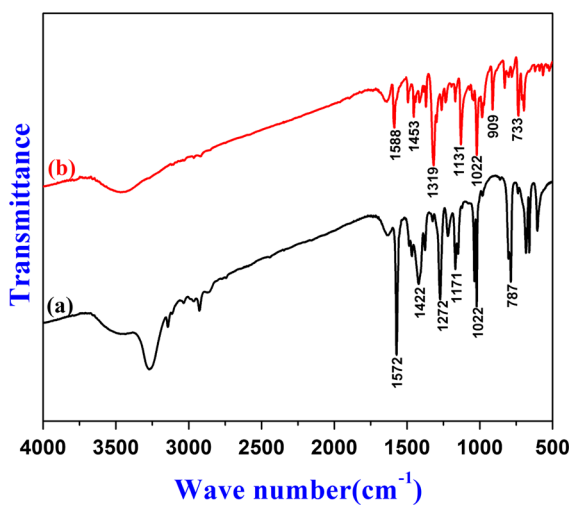

Fig. 1 FTIR spectra of (**a**) bdpa and (**b**) $[Cu(bdpa)_2][CuCl_2]$ in solid-state KBr pallet

strongly supports the synthesis of $Cu_{2-x}S$ ($x = 0.03$, 0.2) nanocrystals.

The suitability of SP for the preparation of copper sulfide NCs is further envisaged by thermogravimetric (TG) analysis. The TGA thermogram of $[Cu(bdpa)_2\text{-}CuCl_2]$ shows a three-step decomposition pattern as shown in Fig. 3. The complex undergoes significant weight loss in first two stages 16.6 % (calculated value 17.04 %) and 14.7 % (calculated value 15.15 %) between temperatures 140 and 300 °C due to the loss of $–SCH_2Ph$ and $–CH_2Ph$ fragments, respectively. The another major loss 37.31 % over a temperatures range 300–430 °C is the decomposition of all remaining organic groups giving a residue 31.39 %, which is close to the value calculated for the mass percentage of bulk Cu_2S_3 (30.89 %). The possible steps for thermal decomposition of $[Cu(bdpa)_2][CuCl_2]$ are shown in Scheme 1.

The reaction temperature for the solvothermal decomposition of the SP is maintained at 180 °C (above the decomposition temperature) expecting entire loss of all organics leading to the formation of copper sulfide. In our experiment, the higher reaction temperature than the decomposition temperature of the precursor is considered with heating duration of 1 h in each set of experiment taking same concentration of SP.

In a simple one-step process, the SP is subjected to decompose in a coordinating solvent. The selective synthesis of copper(I) sulfide was possible using coordinating solvent. The temperature is maintained at 180 °C which is far above the SP's decomposition temperature to ensure the complete conversion of SP into particles. It is also note worthy that no surfactant is used in this process. To this end, the process is quite

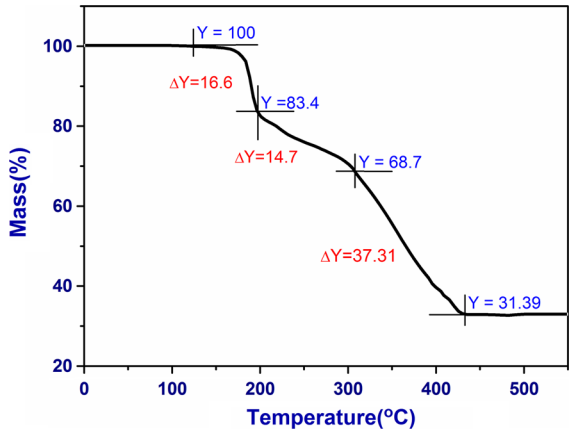

Fig. 3 TGA curve of SP under N_2 atmosphere

green with respect to other reported methods. The solvent molecules serve the purpose of particle stabilization. The change in solvent merely alters the composition of copper(I) sulfide NCs. Bidentate solvent EN and EG furnished copper-deficient $Cu_{1.97}S$ (Djurleite), whereas mono dentate amine HH (NH_2NH_2) confirms the formation of $Cu_{1.8}S$. It is quite surprising that the Cu(I) sulfide NCs thus obtained are smaller in size than Bohr radius without using any strong external surfactant. The NCs are quite stable for several weeks with respect to photo and air oxidation. The crystallinity and phase structure of the copper sulfide nanocrystals were examined by X-ray diffraction technique. Figure 4a–c represents the XRD pattern of the synthesized copper sulfide materials from the precursor complexes by solvothermal process using EG, EN, and HH solvents, respectively. Fairly intense peaks observed in all the cases are indicative of their good crystallinity. The high-intensity diffraction

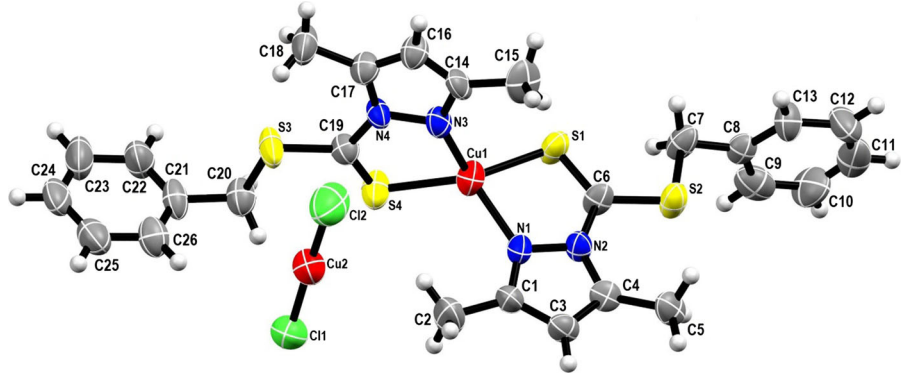

Fig. 2 ORTEP diagram of SP, $[Cu(bdpa)_2][CuCl_2]$

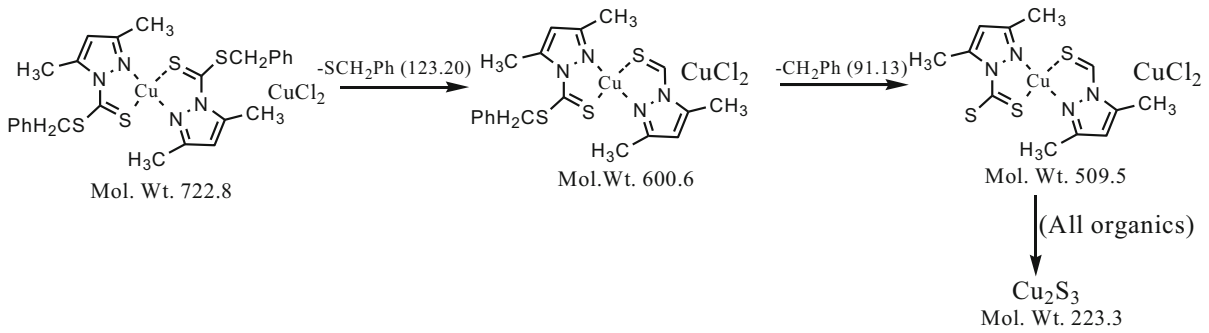

Scheme 1 Thermal decomposition pattern of SP

peaks at 38.06°, 47°, 48.9°, and 55.1° corresponding to plane <5 6 1> , <8 3 5> ,<12 0 4> , and <3 6 6> , respectively, in the spectrum of the samples obtained from EG (Fig. 4a) and EN (Fig. 4b) match well with the JCPDS reference file for copper-deficient $Cu_{1.97}S$ phase (JCPDS 20-0365). The key difference in distinguishing the $Cu_{1.97}S$ phase from Cu_2S is the peak at ~46° rather than peak at 45° (Cu_2S phase) (Zhao et al. 2009). The absence of any intensity peak in the 2θ range 37°–38° in the diffractogram of the sample obtained from HH (Fig. 4c) and the presence of the diffraction peaks at 47.33°, 48.9°, 54.7°, and 56.17° corresponding to plane <0 1 20> , <1 1 9> , <1 1 15> , and <2 0 8> , respectively, indicate mainly the formation of $Cu_{1.8}S$ phase (JCPDS card number 47-1748) rather than $Cu_{1.97}S$. The key difference in distinguishing the $Cu_{1.97}S$ phase from $Cu_{1.8}S$ is the peak at ~37°. However, the additional diffraction

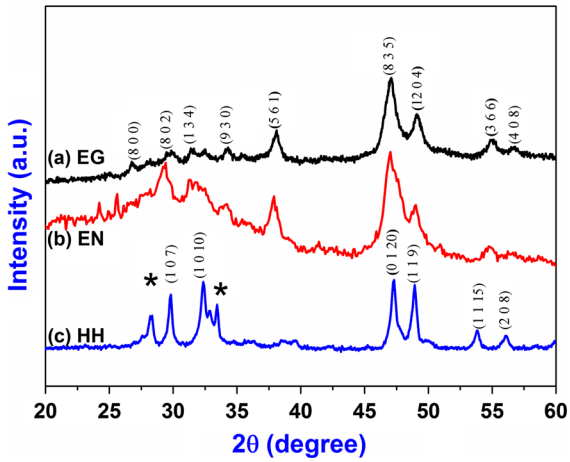

Fig. 4 Powder XRD pattern of copper(I) sulfide NCs synthesized from **a** EG, **b** EN, and **c** HH

peaks at lower 2θ values (indicated as * in Fig. 4c) and peaks at 42° and 51° for sample from EN (Fig. 4b) appearing with appreciable intensity might be due to the presence of trace amount of impurity phase of covellite (CuS) (Zhao et al. 2009). So, the careful investigation of the XRD spectra obtained from different solvents leads to a conclusion that the change in composition of the copper(I) sulfide can be prepared in this precursor route by simple variation of solvent keeping other reaction conditions constant.

The morphologies of copper(I) sulfide nanoparticles obtained from different solvents were investigated by SEM (Fig. 5). In Fig. 5a, b, the SEM images of sample obtained from EG at 180 °C show $Cu_{1.97}S$ microstructure composed of irregular hexagonal particles. As shown in Fig. 5c, d, the morphology of the samples obtained from EN at 180 °C is predominantly large plates with smooth surfaces. It can be assumed that each large plate comprised a large number of stacked hexagonal-shaped small platelets of $Cu_{1.97}S$ NCs with high degree of internal void space. In Fig. 5e, f, the SEM images of the sample obtained from HH at 180 °C shows a flower-like microstructure composed of hexagonal platelets of $Cu_{1.8}S$ NCs with internal grooves and void spaces. The presence of grooves in the surfaces of microstructures and the internal space between agglomerated stacked hexagonal platelets ascertained the high catalytic reactivity through coarse surface of $Cu_{1.8}S$. The details of the surface activity study are discussed later.

The energy-dispersive X-ray spectrum (EDX) was carried out during SEM analysis in EG solvent which shows the Cu:S ratio 2.1:1 which indicates nearly Cu_2S stoichiometry in the sample as shown in Fig. 6. The presence of oxygen in EDX spectrum shows the adsorption of air on the porous groove of the particles

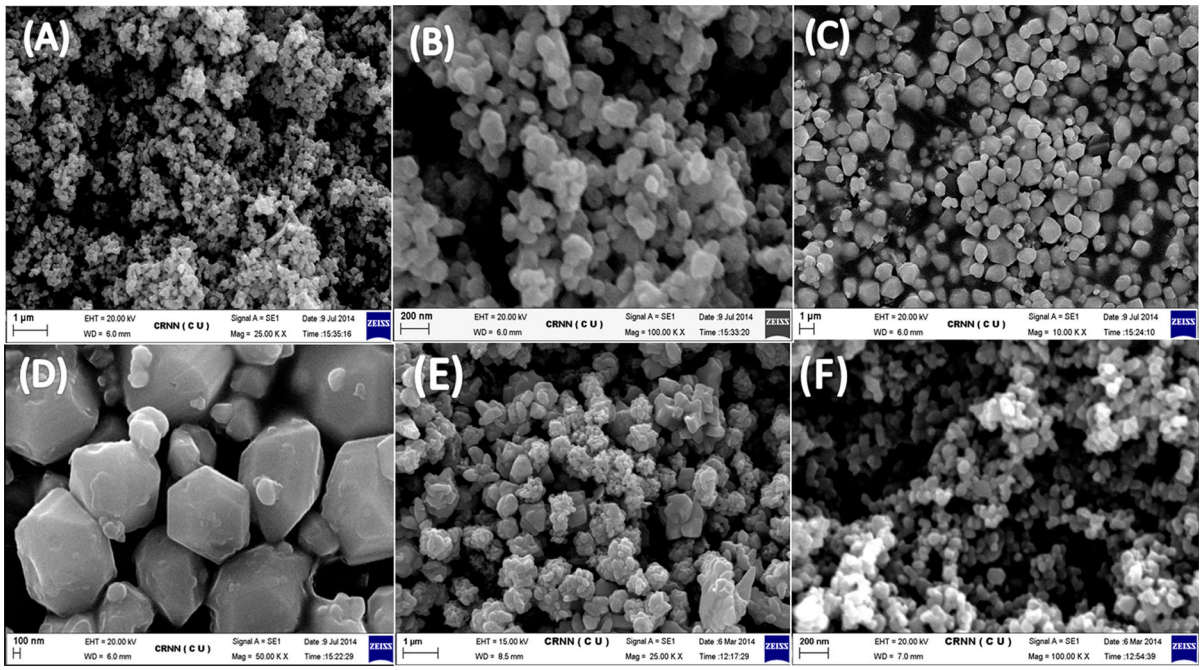

Fig. 5 SEM images of copper(I) sulfide NCs: **a**, **b** from EG; **c**, **d** from EN and **e**, **f** from HH

or the presence of little oxidized copper sulfide species.

The morphologies and size of the synthesized copper(I) sulfide NCs were carried out by transmission electron microscope (TEM). Spherical morphologies with average diameter of 15–18 nm were observed in the sample obtained from EG and EN. Figure 7a, b shows the nearly spherical images of copper(I) sulfide NCs synthesized from EG at 180 °C. Figure 7c, d also indicates the spherical morphology of the nanoparticles obtained from EN at 180 °C. A magnified view in Fig. 7d of a spherical particle clearly demonstrated the presence of the lattice fringe with a spacing 0.33 nm corresponding to (110) lattice plane of hexagonal $Cu_{1.97}S$. Figure 7e, f shows the hexagonal platelets of the samples obtained from HH with average length 60 nm which are greater than the sample size obtained from EG and EN (Table 1). The statistical average diameter and length of the synthesized copper(I) sulfide NCs are shown in Fig. 8. The formation of a hexagonal crystal structure of $Cu_{2-x}S$ ($x = 0.03, 0.2$) is reasonable because the reaction temperature is higher than its phase transition temperature (103.5 °C), at which metastable low chalcocite (monoclinic) undergoes a phase transition to high chalcocite Cu_2S. Etching in the surface of NCs is observed in the

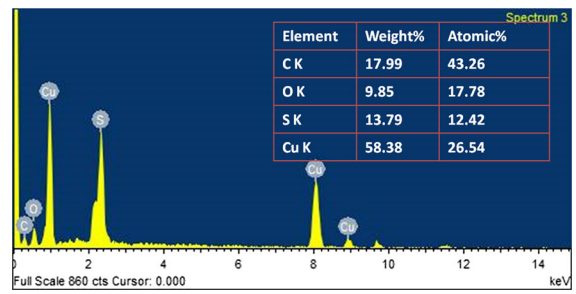

Fig. 6 EDX spectrum of copper sulfide NCs prepared from EG at 180 °C

samples when HH is used as solvent. This phenomenon is common for the particles when HH is used in the thermolysis of the precursor (Fig. S1). The reason may be due to the higher corrosive nature of HH. The size and morphology of the copper-deficient copper(I) sulfides ($Cu_{2-x}S$, $x = 0.03, 0.2$) are dependent both of the SP's structure and the solvent. The SP helps to form only copper(I) sulfide and the solvent polarity and coordination pattern influence the stoichiometry and morphology. Being strong coordinating solvents, EN and EG effectively circumfuse the particles facilitating the formation of spherical shape where weakly coordinating solvent HH weakly covers

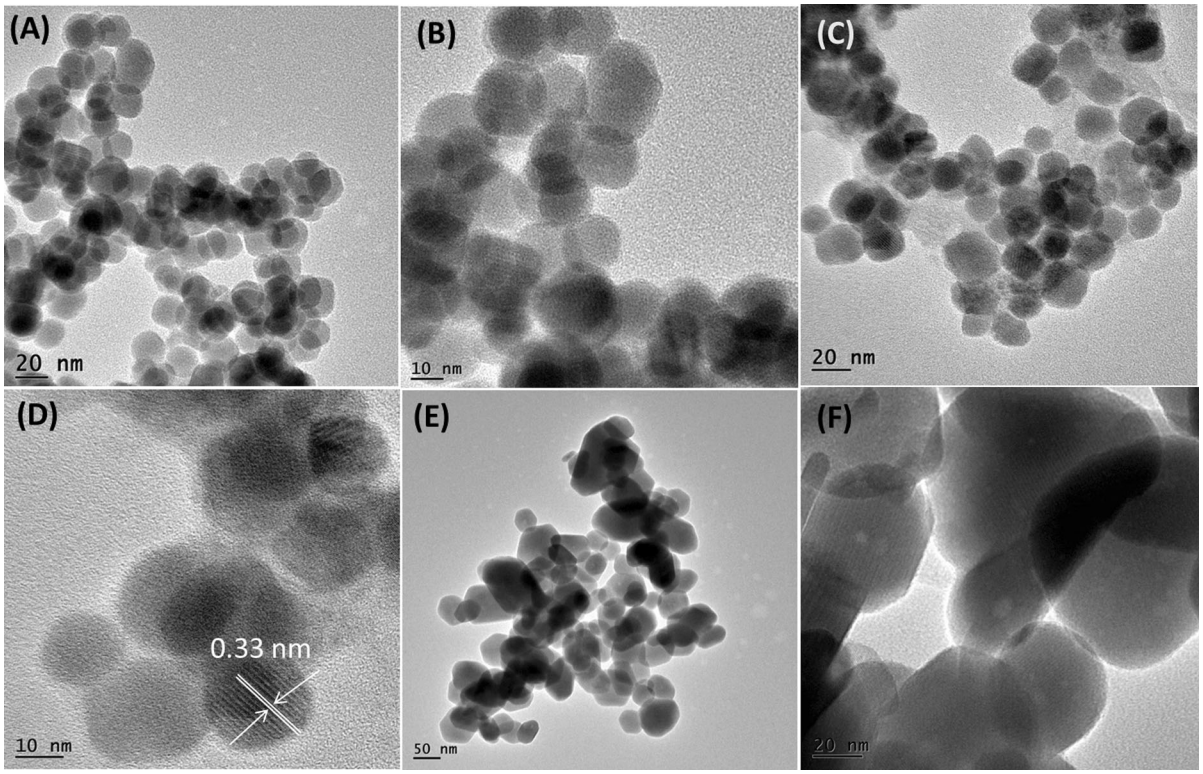

Fig. 7 TEM and HRTEM of copper(I) sulfide NCs: **a**, **b** from EG; **c**, **d** from EN and **e**, **f** from HH solvent at 180 °C

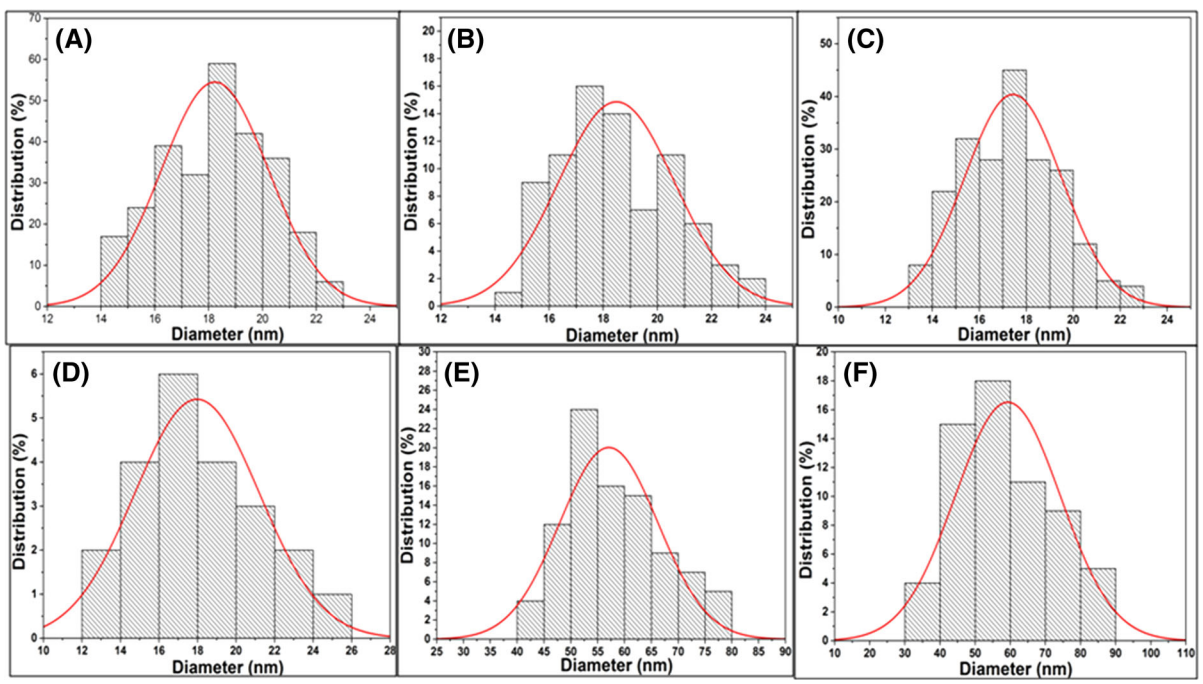

Fig. 8 Statistical diameters of copper(I) sulfide NCs from TEM images: **a**, **b** from EG; **c**, **d** from EN and length of copper(I) sulfide NCs **e**, **f** from HH solvent at 180 °C

the surface of the seed particles leading to grow anisotropically to hexagonal $Cu_{1.8}S$.

The chemical state and composition of the sample Cu_2S were determined by X-ray photoelectron spectroscopy (XPS). The value of binding energy was calibrated by C(1 s) peak (281.69 eV) as the internal standard. Figure 9 shows the typical survey spectrum of copper(I) sulfide NCs obtained from EG at 180 °C. The core peaks of Cu 2p appear at ~950 eV (2 $p_{1/2}$) and ~930 eV (2 $p_{3/2}$). The Cu 2p signals reach its maximum value at a binding energy of 930 eV with a split orbit of 20 eV which is indicative to the presence of Cu(+1) or Cu(0) rather than Cu(+2) in the sample. Another survey on S 2p region shows the presence of doublet peaks at ~160 eV which can be assigned to the Cu–S– form. The features of XPS spectrum prove the presence of Cu(+1) in the sample.

The optical absorption spectra of the samples are shown in Fig. 10. A broad peak in the visible region is observed with a trail in the long wavelength direction that can be turned to cover the whole visible range. The absorption never reaches to zero intensity but rises to the longer wave length. The sample obtained from EG (Fig. 10a) reaches a minimum around 650 nm and then it rises for longer wavelength which is stronger than the samples obtained from EN and HH due to free carrier intraband absorption [40]. However, the rises are not so sharp for the samples obtained from EN and HH. The optical band gap is determined using Tauc's equation $(\alpha h\upsilon)^n = A(h\upsilon - E_g)$, where α is the absorption coefficient, $h\upsilon$ is the photon energy, A is a constant, E_g is the band gap, and n is either 1/2 for an indirect transition or 2 for a direct transition. Thus, a plot of $(\alpha h\upsilon)^2$ vs $(h\upsilon)$ for direct band gap copper sulfide gives a straight line whose intercept on the energy axis refers the energy gap (E_g). As shown in Fig. 11, the E_g values 1.87, 2.04 and 2.5 eV for the samples synthesized from EG, EN, and HH, respectively, indicate quantum confinement effect in structure.

It is interesting to note that spherical morphology is common when Cu(II)-smdtc (where smdtc = H_2-NNH-C(S)SCH_3) (Bera et al. 2010) and Cu(I)-mdpa (where mdpa is methyl 3,5-dimethyl-pyrazole-1-carbodithioate) (Mondal et al. 2015) were thermolyzed in chelating solvents like EN and EG. Both the Cu(II)-smdtc and Cu(I)-mdpa produce methane thiol (CH_3-SH) fragment during thermolysis. It may be concluded that thermodynamic spherical morphology of copper sulfide NCs is common in the solvothermal decomposition of SPs derived from smdtc and sbdtc. But a tendency for an anisotropic growth is resulted with fewer passivation of the fragments (RSH) and less wettability of the solvent used in the thermolysis. The hexagonal morphology of the nanoparticles in the present study with HH can be attributed by the combined effects of less surface passivation by $PhCH_2SH$ and shorter wettability of HH than bivalent solvents like EN and EG. Being a larger thiol, $PhCH_2SH$ provides lesser surface passivation than CH_3SH. So, larger size of nanoparticles is thus quite expected when SP contains $–SCH_2Ph$ moiety. The mechanistic pathway is shown in Scheme 2.

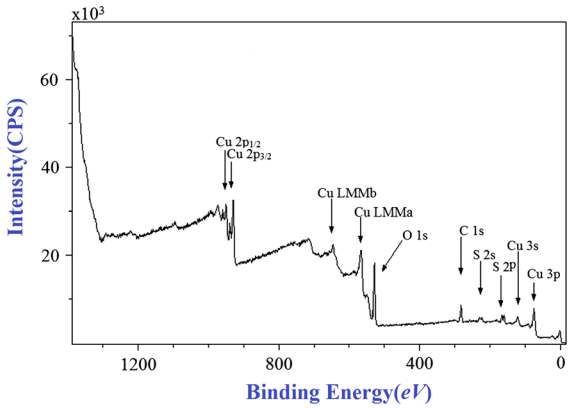

Fig. 9 XPS spectrum of copper(I) sulfide NCs prepared from SP using EG solvent at 180 °C

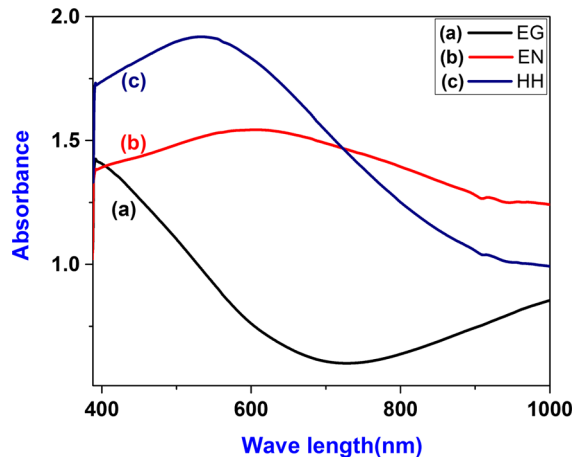

Fig. 10 UV–Vis absorption spectrum of copper(I) sulfide NCs and corresponding band gap energy prepared from **a** EG, **b** EN, and **c** HH solvent

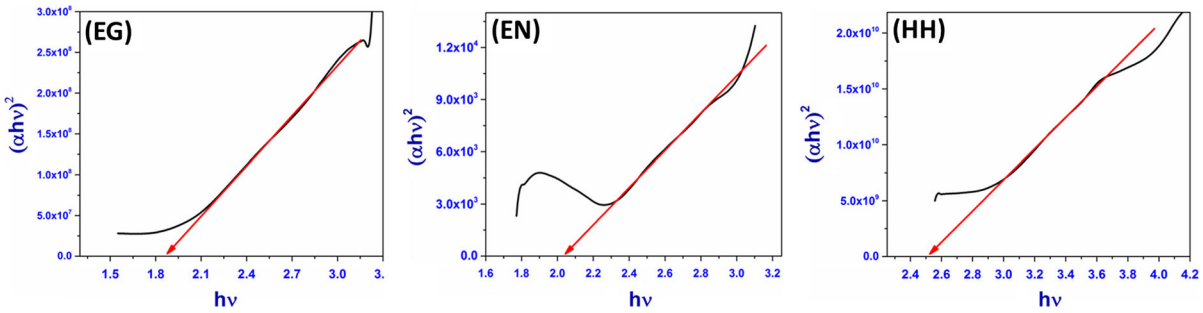

Fig. 11 Plot of $(\alpha h\nu)^2$ vs $(h\nu)$

In textile industries, various dyes are used, which are very stable organic aromatic compounds, low biodegradable and major portion are environmental pollutants. The waste water from textile mills containing these dyes causes serious contamination on natural water. These dyes not only impart colors to water sources but also damage living organisms by stopping the re-oxygenation capacity of water, blocking sunlight, and therefore disturbing the natural growth activity of aquatic life (Song et al. 2010; Wang 2008; Partain et al. 1983). Thus, the color removal of textile waste water is a major environmental concern (Khehra et al. 2005). Certain semiconducting NCs having band gap values 1.8–2.5 eV show photocatalytic activities. The NCs decompose the harmful organic molecules into small benign one. Semiconducting materials when irradiated in visible light absorb photon energy greater than their band gap; consequently, electron–hole pairs are produced which subsequently transfer to the surface of the crystal. This electrons ($\bar{e}$) and holes (h^+) react with H_2O and molecular O_2, producing $\cdot OH$ and $\cdot O_2^-$ radicals, respectively. These free radicals are responsible for catalytic decomposition of organic dyes. In the present work, we chose organic dyes Congo Red (CR) and Methylene Blue (MB) to testify the photocatalytic activity of the synthesized semiconducting $Cu_{2-x}S$ ($x = 0.03,\ 0.2$) because these fluorescence dyes are commonly used in textile, photographic, and photochemical industries. The experiment was carried out by using aqueous solution of CR and MB solution under visible light with out and with $Cu_{2-x}S$ ($x = 0.03,\ 0.2$) NCs. It is observed that the absence of catalyst under visible light irradiation as well as the presence of catalyst in the dark indicates no appreciable degradation of both the dyes even after 1.5 h. In the presence of catalyst and light, the system shows ~87 % degradation of dye molecules. Figure 12 shows the time-dependent UV–Vis spectral change of CR and MB solution in the presence of $Cu_{2-x}S$ ($x = 0.03,\ 0.2$) NCs under the irradiation of light for 90 min and 80 min, respectively. All the experiments were carried out with 50 mL aqueous solution of each 6.2×10^{-5} (M) CR and 5.0×10^{-5} (M) MB taken in a 100 mL beaker with 15 mg $Cu_{2-x}S$ ($x = 0.03,\ 0.2$) under a 250 W indoor fluorescent lamp as visible light source. The solutions were stored in dark place for 30 min to reach adsorption desorption equilibrium and then initial absorption was measured in UV–Vis spectrophotometer. The absorption of the sample was again measured after exposition in visible light at 10-min interval by taking 3 mL of solution with constant stirring followed by centrifugation.

The characteristics absorption peaks that appeared at 480 nm and 650 nm for CR and MB, respectively, gradually decreased without giving any additional absorption peak. The % of degradation of dyes is calculated using following relationship: $D\ (\%) = (C_0 - C_t)/C_0 \times 100$, where C_0 and C_t are the concentrations at initial and any time t of the dyes, respectively.

A maximum degradation of CR (85 %) is observed after 90-min visible light irradiation where the maximum degradation of MB (87 %) is recorded after 80 min. The photodegradation profile picture is given in Fig. 13.

The dye degradation follows first-order kinetics and obeys the rate equation $\ln (C_t/C_0) = kt$, (k is rate constant) in both the cases. The rate constant values are 14.74×10^{-3} and 16.91×10^{-3} min^{-1} for CR and MB dyes, respectively, and the corresponding figures are provided in the supplementary information (Fig. S2).

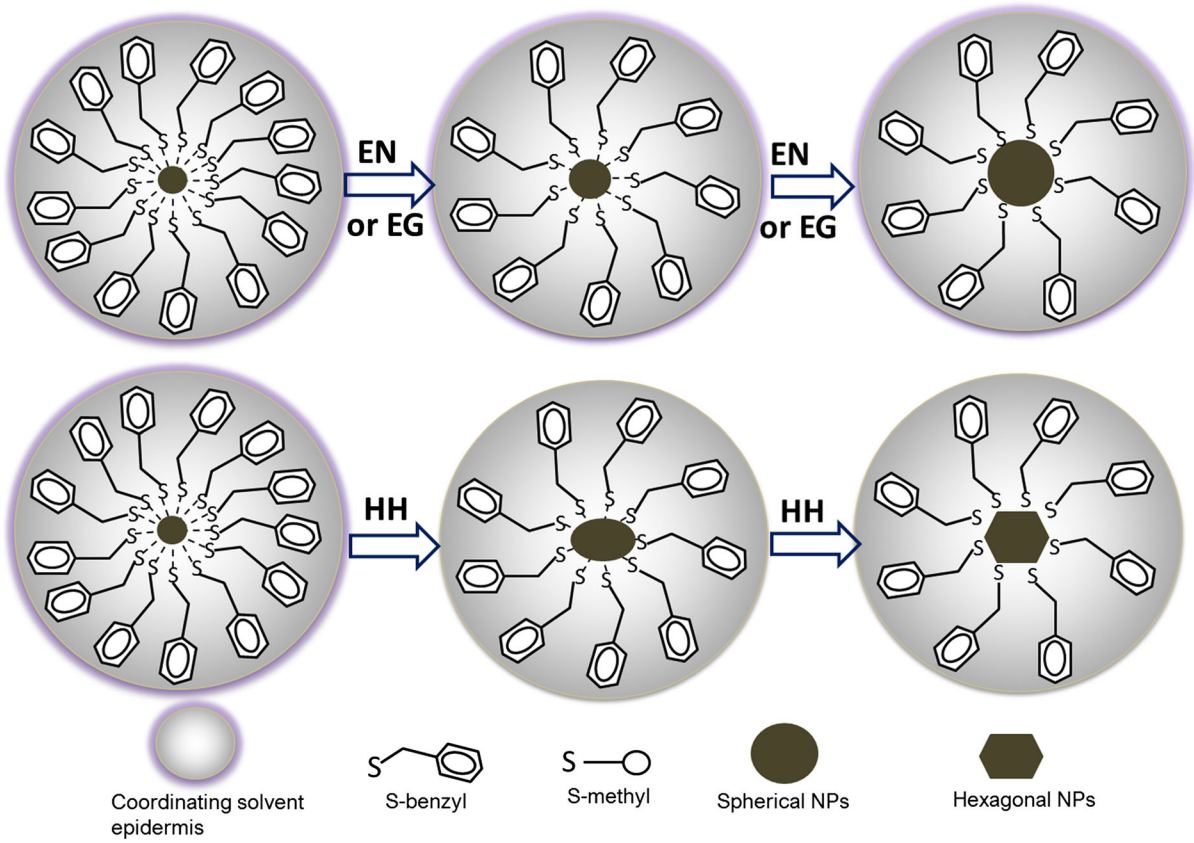

Scheme 2 Proposed formation mechanism of hexagonal-shaped copper(I) sulfide NCs

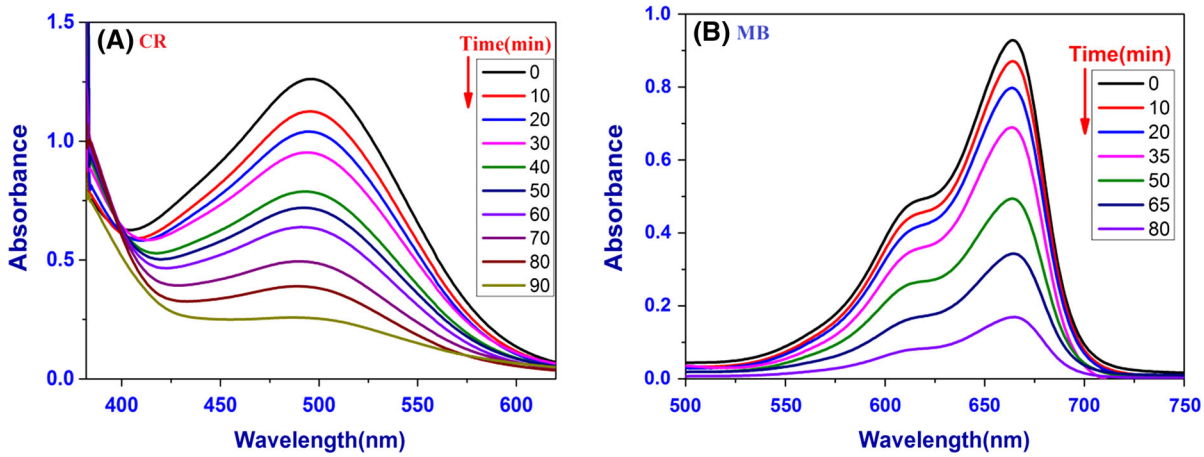

Fig. 12 UV–Vis spectral change during photodegradation of **a** CR and **b** MB, both samples are prepared from EG solvent

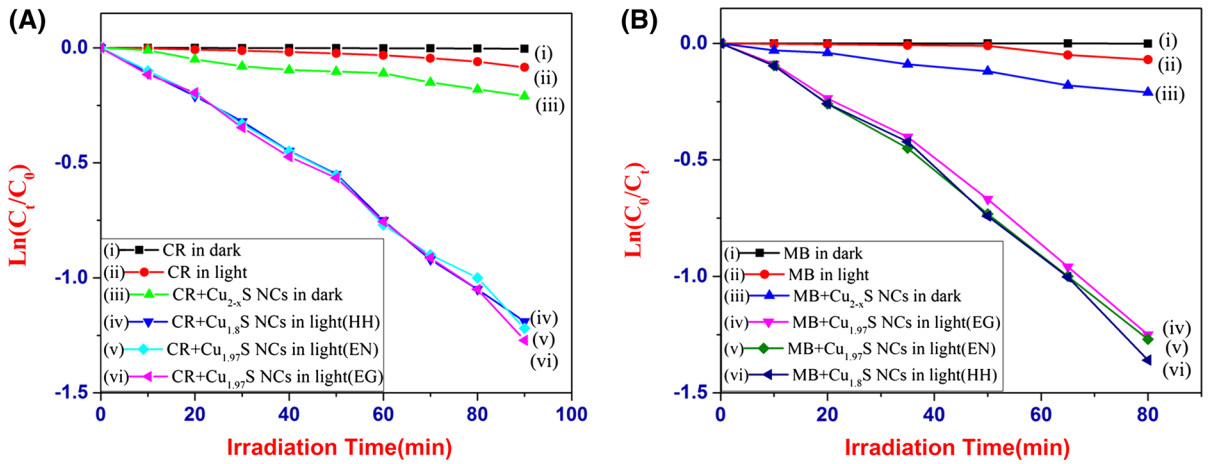

Fig. 13 Photodegradation of CR (**a**) and MB dyes (**b**) under various conditions

Conclusions

A pyrazolyl-derived thiolate NS-chelate is used to synthesize air-stable Cu(I) complex $[Cu(bdpa)_2][CuCl_2]$, where bdpa is benzyl 3,5-dimethyl-pyrazole-1-carbodithioate. The complex is used as single-source precursor (SP) for the selected synthesis of $Cu_{2-x}S$ ($x = 0.03,\ 0.2$) nanocrystals (NCs) following thermal decomposition in ethylene glycol (EG), ethylene diamine (EN), and hydrazine hydrate (HH). The +1 oxidation state of the SP facilitates the selective formation of copper-deficient $Cu_{2-x}S$ ($x = 0.03, 0.2$) NCs of size 15 nm. Chelating solvents such as EN and EG have stronger interaction with the nucleated surface of seeded crystals than nonchelating HH which leads to spherical shape of $Cu_{1.97}S$ NCs. The hexagonal plate morphology of $Cu_{1.8}S$ is resulted when the SP is decomposed in the HH solvent. As is observed in the SEM, the porous architecture of the product might have been effective photocatalyst for organic molecules. Optical band gap values 1.8–2.5 eV of the sample are indicative of quantum confinement effect. The $Cu_{2-x}S$ ($x = 0.03, 0.2$) NCs are found to be an excellent catalyst for photodegradation of organic dyes Congo Red (CR) and Methylene Blue (MB). Further studies on heterocycle-based precursor for the selective synthesis of low-valence metal sulfide nanoparticles can be explored to establish the structure and activity relationship between precursor complexes and derived particles.

Acknowledgments We gratefully acknowledge the research grant from CSIR, Government of India [Grant No. 1(2534)/11/EMR-II] and UGC, Government of India [F 42-280/2013(SR)]. We are thankful to the people of CRNN, Calcutta University for TEM and SEM analysis.

References

Ali MA, Mirza AH, Ting WY, Hamid AHSA, Bernhardt PV, Butcher RJ (2012) Mixed ligand nickel(II) and copper(II) complexes of tridentate ONS and NNS ligands derived from S-alkyldithiocarbazate with saccarinate ion as co-ligand. Polyhedron 48:147–173

Bera P, Kim CH, Seok SI (2008) Synthesis, spectroscopic characterization and thermal behavior of cadmium(II) complexes of S-methyldithiocarbazate (SMDTC) and S-benzyldithiocarbazate (SBDTC): X-ray crystal structure of $[Cd(SMDTC)_3]\ 2NO_3$. Polyhedron 27:3433–3437

Bera P, Kim CH, Seok SI (2010) Synthesis of nanocrystalline CdS from cadmium(II) complex of S-benzyl dithiocarbazate as a precursor. Solid State Sci 12:1741–1747

Chen L, Xia YD, Liang XF, Yin KB, Yin J, Liu ZG, Chen Y (2007) Nonvolatile memory devices with Cu_2S and Cu-Pc bilayered films. Appl Phys Lett 91:073511–073513

Du XS, Yu ZZ, Dasari A, Ma J, Meng YZ, Mai YW (2006) Facile synthesis and assembly of Cu2S nanodisks to corncoblike nanostructures. Chem Mater 18:5156–5158

Ghahremaninezhad A, Asselin E, Dixon DG (2011) Electrodeposition and growth mechanism of copper sulfide nanowires. J Phys Chem C 115:9320–9334

Gonçalves AP, Lopes EB, Casaca A, Dias M, Almeida M (2008) Growth of CuS platelet single crystals by the high-temperature solution growth technique. J Cryst Growth 310:2742–2745

Gong JY, Yu SH, Qian HS, Luo LB, Liu XM (2006) Acetic acid-assisted solution process for growth of complex copper sulfide microtubes constructed by hexagonal nanoflakes. Chem Mater 18:2012–2015

Gorai S, Ganguli D, Chaudhuri S (2005) Synthesis of copper sulfides of varying morphologies and stoichiometries

controlled by chelating and nonchelating solvents in a solvothermal process. Cryst Growth Des 5:875–877

Haram SK, Mahadeshwar AR, Dixit SG (1996) Synthesis and characterization of copper sulfide nanoparticles in Triton-X 100 water-in-oil microemulsions. J Phys Chem 100:5868–5873

He Y, Yu X, Zhao X (2007) Synthesis of hollow CuS nanostructured microspheres with novel surface morphologies. Mater Lett 61:3014–3016

Jiang X, Xie Y, Lu J, He W, Zhu L, Qian Y (2000) Preparation and phase transformation of nanocrystalline copper sulfides (Cu_9S_8, Cu_7S_4 and CuS) at low temperature. J Mater Chem 10:2193–2196. doi:10.1039/B002486O

Khehra MS, Saini HS, Sharma DK, Chadha BS, Chimni SS (2005) Comparative studies on potential of consortium and constituent pure bacterial isolates to decolorize azo dyes. Water Res 39(20):5135–5141

Lai C-H, Lu M-Y, Chen L-J (2012) Metal sulfide nanostructures: synthesis, properties and applications in energy conversion and storage. J Mater Chem 22:19–30. doi:10.1039/C1JM13879K

Larsen TH, Sigman M, Ghezelbash A, Doty RC, Korgel BA (2003) Solventless synthesis of copper sulfide nanorods by thermolysis of a single source thiolate-derived precursor. J Am Chem Soc 125:5638–5639

Li S, Wang HZ, Xu WW, Si HL, Tao X, Lou S, Du Z, Li L (2009) Synthesis and assembly of monodisperse spherical Cu_2S nanocrystals. J Coll Interf Sci 330:483–487

Lin MC, Lee MW (2011) $Cu_{2-x}S$ quantum dot-sensitizedsolar cells. Electrochem Commun 13:1376–1378

Liu ZP, Xu D, Liang JB, Shen JM, Zhang SY, Qian TY (2005) Growth of Cu_2S ultrathin nanowires in a binary surfactant solvent. J Phys Chem B 109:10699–10704

Lou W, Chen M, Wang X, Liu W (2007) Size control of monodisperse copper sulfide faceted nanocrystals and triangular nanoplates. J Phys Chem C 111:9658–9663

Lu QY, Gao F, Zhao DY (2002) One-step synthesis and assembly of copper sulfide nanoparticles to nanowires, nanotubes, and nanovesicles by a simple organic amine-assisted hydrothermal process. Nano Lett 2:725–728

Malyarevich AM, Yumashev KV, Posnov NN, Mikhailov VP, Gurin VS, Prokopenko VB, Alexeenko AA, Melnichenko IM (2000) Nonlinear optical properties of Cu_xS and $CuInS_2$ nanoparticles in sol–gel glasses. J Appl Phys 87:212

Mondal G, Bera P, Santra A, Jana S, Mondal TN, Mondal A, Seok SI, Bera P (2014) Precursor-driven selective synthesis of hexagonal chalcocite (Cu_2S) nanocrystals: structural, optical, electrical and photocatalytic properties. New J Chem 38:4774–4782

Mondal G, Acharjya M, Santra A, Bera P, Jana S, Pramanik NC, Mondal A, Bera P (2015) A new pyrazolyl dithioate function in the precursor for the shape controlled growth of CdS nanocrystals: optical and photocatalytic activities. New J Chem 39:9487–9496

Mthethwa T, Pullabhotla VSRR, Mdluli PS, Wesley-Smith J, Revaprasadu N (2009) Synthesis of hexadecylamine capped CdS nanoparticles using heterocyclic cadmium dithiocarbamates as single source precursors. Polyhedron 28:2977–2982

Nair PS, Scholes GD (2006) Thermal decomposition of single source precursors and the shape evolution of CdS and CdSe nanocrystals. J Mater Chem 16:467–473

Nyamen LD, Pullabhotla VSR, Nejo AA, Ndifon P, Revaprasadu N (2011) Heterocyclic dithiocarbamates: precursors for shape controlled growth of CdS nanoparticles. New J Chem 35:1133–1139

Nyamen LD, Revaprasadu N, Pullabhotla RVSR, Nejo AA, Ndifon PT, Malik MA, O'Brien P (2013) Synthesis of multi-podal CdS nanostructures using heterocyclic dithiocarbamato complexes as precursors. Polyhedron 56:62–70

Partain LD, Mcleod PS, Duisman JA, Peterson TM, Sawyer DE, Dean CS (1983) Degradation of a Cu(x)S/CdS solar cell in hot, moist air and recovery in hydrogen and air. J Appl Phys 54:6708–6720

Reijnen L, Meester B, Goossens A, Schoonman J (2003) Atomic layer deposition of Cu_xS for solar energy conversion. Chem Vap Depos 9:15–20. doi:10.1002/cvde.200290001

Roy P, Srivastava SK (2006) Hydrothermal growth of CuS nanowires from Cu − Dithiooxamide, a novel single-source precursor. Cryst Growth Des 6:1921–1926

Roy P, Srivastava SK (2007) Low-temperature synthesis of CuS nanorods by simple wet chemical method. Mater Lett 61:1693–1697

Sagade AA, Sharma R, Sulaniya I (2009) Enhancement in sensitivity of copper sulfide thin film ammonia gas sensor: effect of swift heavy ion irradiation. J Appl Phys 105:043701–043708

Sakamoto T, Sunamura H, Kawaura H, Hasegawa T, Nakayama T, Aono M (2003) Nanometer-scale switches usingcopper sulphide. Appl Phys Lett 82:3032–3034

Shen S, Zhang Y, Peng L, Xu B, Du Y, Deng M, Xu H, Wang Q (2011) Generalized synthesis of metal sulfide nanocrystals from single-source precursors: size, shape and chemical composition control and their properties. Cryst Eng Com 13:4572–4579

Sigman MB, Ghezelbash A, Hanrath T, Saunders AE, Lee F, Korgel BA (2003) Solventless synthesis of monodisperse Cu_2S nanorods, nanodisks, and nanoplatelets. J Am Chem Soc 125:16050–16057

Song Y-L, Li J-T, Bo Bai (2010) TiO_2-assisted photodegradation of direct blue 78 in aqueous solution in sunlight. Water Air Soil Pollut 213:311–317

Thongtem T, Phuruangrat A, Thongtem S (2009) Formation of CuS with flower-like, hollow spherical, and tubular structures using the solvothermal-microwave process. Curr Appl Phys 9:195–200

Wang S (2008) A comparative study of Fenton and Fenton-like reaction kinetics in decolourisation of wastewater. Dyes Pigm 76(3):714–720

Wang H, Zhang J, Zhao X, Xu S, Zhu JJ (2002) Preparation of copper monosulfide and nickel monosulfide nanoparticles by sonochemical method. J Mater Lett 55:253–258

Wu CY, Yu SH, Chen S, Liu GN, Liu BH (2006) Large scale synthesis of uniform CuS nanotubes in ethylene glycol by a sacrificial templating method under mild conditions. J Mater Chem 16:3326–3331

Wu Y, Wadia C, Ma W, Sadtler B, Alivisatos AP (2008) Synthesis and photovoltaic application of copper(I) sulfide nanocrystals. Nano Lett 8:2551–2555

Xie Y, Riedinger A, Prato M, Casu A, Genovese A, Guardia P, Sottini S, Sangregorio C, Miszta K, Ghosh S, Pellegrino T, Manna L (2013) Copper sulfide nanocrystals with tunable composition by reduction of covellite nanocrystals with Cu^{+} ions. J Am Chem Soc 135:17630–17637

Yan HJ, Wang WZ, Xu HL (2008) A micro-interface route to CuS superstructure composed of intersectional nanoplates. J Cryst Growth 310:2640–2643

Zhang S, Ning J, Zhao L, Liu B, Zou B (2010) Facile synthesis and assembly of CuS nano-flakes to novel hexagonal prism structures. J Cryst Growth 312:2060–2064

Zhao Y, Pan H, Lou Y, Qiu X, Zhu JJ, Burda C (2009) Plasmonic $Cu_{2-x}S$ nanocrystals: optical and structural properties of copper-deficient copper(I) sulfides. J Am Chem Soc 131:4253–4261

Zhao L, Tao F, Quan Z, Zhou X, Yuan Y, Hu J (2012) Bubble template synthesis of copper sulfide hollow spheres and their applications in lithium ion battery. Mater Lett 68:28–31